



The Subduction Zone Flow Field from Seismic Anisotropy: A Global View
Maureen D. Long, *et al.*
Science **319**, 315 (2008);
DOI: 10.1126/science.1150809

The following resources related to this article are available online at www.sciencemag.org (this information is current as of January 18, 2008):

Updated information and services, including high-resolution figures, can be found in the online version of this article at:

<http://www.sciencemag.org/cgi/content/full/319/5861/315>

Supporting Online Material can be found at:

<http://www.sciencemag.org/cgi/content/full/319/5861/315/DC1>

This article **cites 25 articles**, 4 of which can be accessed for free:

<http://www.sciencemag.org/cgi/content/full/319/5861/315#otherarticles>

This article appears in the following **subject collections**:

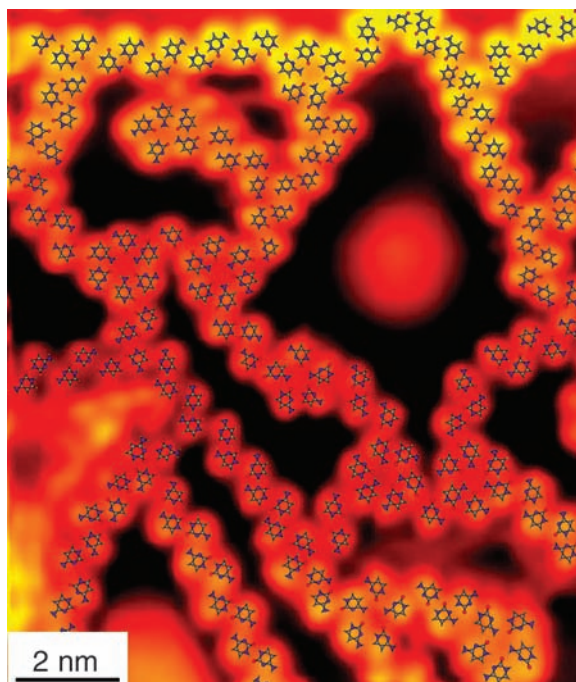
Geochemistry, Geophysics

http://www.sciencemag.org/cgi/collection/geochem_phys

Information about obtaining **reprints** of this article or about obtaining **permission to reproduce this article** in whole or in part can be found at:

<http://www.sciencemag.org/about/permissions.dtl>

Fig. 4. STM image of a “glassy state” of cytosine on Au(111), with an overlay illustrating that a few elementary hydrogen-bonded structural motifs and their possible connections explain the image. Scanning conditions: $I_t = -0.15$ nA, $V_t = -1767$ mV.



the filament, but it also interacts with two molecules of the neighboring filaments through vdW interactions. In the random network we observed, only hydrogen bonding is involved and the majority of the C molecules are bound to only two neighbors through hydrogen bonding. Hence, because of an additional vdW interaction, the binding energy per molecule in relatively large islands of parallel C filaments will be greater than in a random network containing the same number of molecules. This ensures that the ordered arrangement has the lowest energy, and thus it serves as the 2D cytosine ground state.

Because crystalline islands can only survive if they are larger than some critical size, kinetically their formation is highly unlikely. Indeed, upon fast cooling, the formation rate of a large stable crystalline nucleus cannot compete with the formation rate of much smaller structures such as 5- and 6-fold rings, roundabouts, and T junctions—which are energetically the most stable clusters containing small numbers of C molecules—and the system gets trapped in a random network during the first stage of the kinetic process of assembly formation. Thus, this kinetic process leads to a dynamical capture of the 2D fluid upon fast cooling when the available thermal energy in the system becomes insufficient to facilitate escape from the local order of the liquid state into the ground crystalline state.

We thus conclude that, despite the lack of periodicity in the random cytosine network, we have revealed that only a few elementary structural motifs exist through which C molecules bind to each other, and yet very complex structures can be formed from these structural building blocks. The present cytosine model system is kinetically trapped in a disordered state, much like glass is trapped in the amorphous state, because it would need to

overcome prohibitively large energy barriers to move away from it. Examples of glass-forming systems where the constituents are molecules that can form hydrogen bonds in one of their ends but interact only weakly through their other parts (e.g., ethanol) are known in the literature (16). Our results may reveal an interesting route for studying the structure of organic glasses: performing a systematic search of particularly stable motifs and their possible interconnections.

The structure we describe here is similar to a continuous random network, where the constituents of the network are not individual atoms or molecules but instead consist of a small number of supramolecular elementary motifs, some of

which present medium-range order. The identification of such structural motifs would not have been possible without the proper choice of a model system and the use of STM to reveal the nanoscale order.

References and Notes

1. R. Zallen, *The Physics of Amorphous Solids* (Wiley-VCH, Weinheim, Germany, ed. 1, 2004).
2. S. C. Moss, J. F. Graczyk, *Phys. Rev. Lett.* **23**, 1167 (1969).
3. A. van Blaaderen, P. Wiltzius, *Science* **270**, 1177 (1995).
4. E. R. Weeks, J. C. Crocker, A. C. Levitt, A. Schofield, D. A. Weitz, *Science* **287**, 627 (2000).
5. J. V. Barth, *Annu. Rev. Phys. Chem.* **58**, 375 (2007).
6. F. Rosei *et al.*, *Prog. Surf. Sci.* **71**, 95 (2003).
7. R. Otero, F. Rosei, F. Besenbacher, *Annu. Rev. Phys. Chem.* **57**, 497 (2006).
8. R. Otero *et al.*, *Angew. Chem. Int. Ed.* **44**, 2270 (2005).
9. M. Furukawa, H. Tanaka, T. Kawai, *J. Chem. Phys.* **115**, 3419 (2001).
10. Q. Chen, N. V. Richardson, *Nat. Mater.* **2**, 324 (2003).
11. L. M. A. Perdigo *et al.*, *Phys. Rev. B* **73**, 195423 (2006).
12. R. E. A. Kelly, Y. J. Lee, L. N. Kantorovich, *J. Phys. Chem. B* **109**, 22045 (2005).
13. M. Schunack *et al.*, *Phys. Rev. Lett.* **86**, 456 (2001).
14. M. Schunack *et al.*, *Phys. Rev. Lett.* **88**, 156102 (2002).
15. N. J. Tao, J. A. DeRose, S. M. Lindsay, *J. Phys. Chem.* **97**, 910 (1993).
16. M. A. Ramos *et al.*, *Phys. Rev. Lett.* **78**, 82 (1997).
17. Supported by an EU individual Marie Curie Fellowship, EU-RTN project Atomic and Molecular Manipulation as a New Tool for Science and Technology, and EU project Picolnside (R.O. and M.L.), and by the Danish Ministry for Science, Technology and Innovation through the iNANO Center, the Danish Research Councils, the Danish National Research Foundation, the Carlsberg Foundation, and UK Engineering and Physical Sciences Research Council grant GR/P01427/01. We thank the Materials Chemistry Consortium for computer time on the HPCx supercomputer.

Supporting Online Material

www.sciencemag.org/cgi/content/full/1150532/DC1

Materials and Methods

References

Movies S1 and S2

14 September 2007; accepted 4 December 2007

Published online 13 December 2007;

10.1126/science.1150532

Include this information when citing this paper.

The Subduction Zone Flow Field from Seismic Anisotropy: A Global View

Maureen D. Long* and Paul G. Silver

Although the morphologies of subducting slabs have been relatively well characterized, the character of the mantle flow field that accompanies subduction remains poorly understood. To analyze this pattern of flow, we compiled observations of seismic anisotropy, as manifested by shear wave splitting. Data from 13 subduction zones reveal systematic variations in both mantle-wedge and subslab anisotropy with the magnitude of trench migration velocity $|V_t|$. These variations can be explained by flow along the strike of the trench induced by trench motion. This flow dominates beneath the slab, where its magnitude scales with $|V_t|$. In the mantle wedge, this flow interacts with classical corner flow produced by the convergence velocity V_c ; their relative influence is governed by the relative magnitude of $|V_t|$ and V_c .

Upon propagation through an anisotropic medium, a shear wave is split into two orthogonally polarized components and accumulates a delay time, δt , between the fast and slow waves; the fast direction, ϕ , and δt are

measured (1, 2). In the upper mantle, anisotropy results from the strain-induced lattice preferred orientation (LPO) of olivine (3–6), so that if the relationship between deformation and LPO is known or inferred, shear wave splitting measure-

ments can provide a direct constraint on the geometry of upper mantle deformation and, if the fabric is not a fossil one, the upper mantle flow field.

Although anisotropy has been found in most subduction zones (e.g., 7–10), a wide variety of splitting behavior is observed, including both trench-parallel and trench-perpendicular ϕ , substantial lateral heterogeneity, and a large range of δt from 0 s to greater than 2 s. Anisotropic structure likely varies throughout the four-layered structure of subduction zones: the slab mantle, the slab, the mantle wedge, and the overlying plate. This complexity makes it difficult to resolve where the anisotropy is originating, and it also limits the ability to construct numerical models of mantle flow with which to compare to observations.

The classical flow model for subduction systems is two dimensional (2D), characterized by corner flow above the slab and entrained flow beneath the slab (e.g., 11). (We use the term “subduction system” to refer to the subduction zone and the surrounding mantle flow.) Assuming A-type (or similar) LPO and the local alignment of the fast direction and the flow direction, this model makes the simple prediction of trench-normal orientations for ϕ for anisotropy originating both in the wedge and below the slab. As is well known, this model fails to account for the dramatic variability in ϕ noted above. Alternative models include trench-parallel flow in the mantle wedge (12), flow induced by crustal foundering (13), trench-parallel flow beneath the subducting slab (14), and transpression due to oblique subduction (15). It has also been proposed that olivine changes from A-type LPO to B-type LPO (thus changing the relationship between anisotropy and strain) as a way to explain trench-parallel fast directions in the mantle wedge while retaining 2D corner flow (16–18). Conditions needed for B-type LPO may be present in portions of the mantle wedge, although A-type [or other fabric types that give the same strain-anisotropy relationship, such as C or E (6)] likely prevails elsewhere in the upper mantle. Each of these explanations has been successful in accounting for local observations in specific subduction zones but none explains the full range of splitting behavior observed globally. We have compiled a global data set of average splitting parameters to reveal broad global trends in splitting behavior in terms of tectonic and kinematic subduction parameters, with the aim of determining the dominant properties of the subduction zone flow field.

Our compilation comes from 26 published studies and new measurements from six permanent stations in the Aleutians, Tonga, and Indonesia, covering 13 subduction zones [see supporting

online material (SOM)]. In regions where both local and teleseismic measurements are available, we characterize the wedge and the subwedge region separately. The data are sufficient to constrain the orientation and magnitude of subwedge anisotropy for 11 subduction zones, and wedge anisotropy for 10 (Fig. 1). We compared average splitting parameters to overriding plate velocity, trench migration rate, the stress state of the overriding plate, subducting plate age, convergence rate, slab depth beneath volcanoes, and slab dip, from previous compilations (19, 20).

The splitting results are relatively simple for the subwedge anisotropic signal (see SOM). Nearly all regions where we identified substantial subwedge splitting exhibit trench-parallel ϕ , although many also show variable orientations (e.g., Japan and South America) (fig. S2). Cascadia is a notable exception, with consistently trench-perpendicular ϕ . We found little or no splitting beneath the Ryukyu or Aleutian wedges, but a large δt (~1 to 2 s) for Tonga and Calabria. One question is whether the anisotropic signature comes primarily from the slab mantle or from the slab itself. Two lines of evidence argue against a primary contribution from the slab:

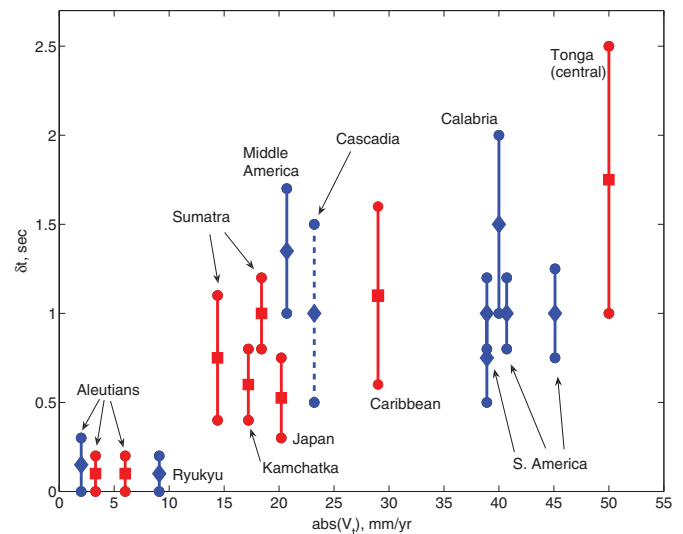
First, the preponderance of trench-parallel ϕ argues for a mechanism related to subduction geometry and not to fossilized anisotropy in the downgoing lithosphere (there is no obvious relationship between fossil spreading direction and ϕ). Second, a slab origin would predict an increase in δt with increasing age (and therefore thickness) of the downgoing lithosphere; we observe no such correlation. Therefore, we interpret the subwedge splitting signal as flow in the slab mantle. Given the physical conditions of the slab mantle, namely low stress, low water content, and relatively high temperature, the LPO is likely to be A-type [or similar (6)], which argues for trench-parallel flow there.

For subduction systems with nearly stationary trenches, there is little or no slab splitting, whereas for systems with migrating trenches, δt tends to increase with the magnitude of trench migration velocity $|V_t|$ (Fig. 2). We propose that slab anisotropy is primarily controlled by 3D return flow, generally parallel to the trench, induced by trench migration, combined with a barrier to entrained flow beneath the slab, likely at either the top or base of the transition zone. As the trench-slab system migrates relative to the



Fig. 1. Summary of available constraints on shear wave splitting in subduction zones. Regions for which robust constraints have been obtained are marked.

Fig. 2. Average slab δt versus $|V_t|$. Retreating trenches are shown with blue diamonds, advancing trenches with red squares. Error bars roughly represent the 95% confidence region on average splitting times (see SOM for further details on error calculations). Cascadia is marked with a dashed line; although it is consistent with the trend with $|V_t|$, its fast directions are not consistent with our preferred model. A linear fit to the data (weighted by errors) produces a relationship of $\delta t = 0.026(|V_t|) + 0.17$; this best-fitting slope is significantly different from zero (the 95% confidence interval on the slope is 0.026 ± 0.07).



Department of Terrestrial Magnetism, Carnegie Institution of Washington, 5241 Broad Branch Road, NW, Washington, DC 20015, USA.

*To whom correspondence should be addressed. E-mail: long@dtm.ciw.edu

upper mantle, subslab mantle is forced around the slab edges and flows parallel to the trench, as has been proposed (14) for South America. The correlation of δt with $|V_t|$ holds regardless of whether the trench is advancing or retreating. We suggest that $|V_t|$ serves as a proxy for the coherence of flow beneath the slab. Subduction systems with fast-moving trenches are more likely to set up a more coherent, larger-scale return flow beneath the slab that results in a larger region of coherent LPO. Similarly, δt , being proportional to the product of intrinsic anisotropy and effective path length, should also be a measure of the length scale of coherent flow, assuming that the intrinsic anisotropy is saturated in the subslab region.

In contrast to the relatively simple trends in subslab anisotropy, anisotropy in the mantle wedge is more difficult to interpret for two reasons. First, the observed splitting patterns in the wedge are much more variable (fig. S3): Many subduction zones exhibit a transition from trench-parallel ϕ close to the trench to trench-perpendicular farther away [e.g., Ryukyu (21), Marianas (10), and Tonga (12)], but a few exhibit the opposite pattern [e.g., Kamchatka (22)]. δt also varies

dramatically between regions: Some wedges are nearly isotropic (e.g., Indonesia and South America), whereas others exhibit large $\delta t > 1$ s (e.g., Ryukyu and Tonga). Second, wedge conditions increase the probability of a change to B-type LPO, which rotates by 90° the expected geometrical relation between strain and ϕ (5).

If 2D corner flow dominated the wedge flow field, one would expect δt to increase with either convergence velocity V_c or with slab dip, which controls path length through the wedge. Yet, there is no such correlation (figs. S4 and S5). After an examination of other plate parameters (e.g., age of subducting lithosphere and stress state of the overriding plate), we find, as with the subslab region, a strong dependence on $|V_t|$. There is a striking relation between δt and $|V_t|$ normalized by V_c , which we define as $V_{\text{norm}} = |V_t|/V_c$ (Fig. 3). Because V_c and $|V_t|$ should govern the strength of 2D corner flow and 3D trench-parallel flow, respectively, this ratio is a measure of the relative importance of these two components in a subduction zone. For subduction systems that are dominated by downdip motion of the slab ($V_{\text{norm}} < \sim 0.2$), δt decreases with increasing V_{norm} . For systems

that are dominated by trench migration ($V_{\text{norm}} > \sim 0.6$), δt tends to increase with increasing V_{norm} , although this pattern is less clear-cut. For systems in between these two regimes, delay times are small.

We hypothesize (Fig. 4) that anisotropy in the wedge is controlled by the competing influences of two flow fields: the 2D corner flow field, which is controlled by viscous coupling between the downgoing slab and the overlying wedge, and the 3D flow field, which is induced by migration of the trench (as in the subslab case). The relative importance of these two flow fields is controlled by the relative magnitudes of $|V_t|$ and V_c . The greater the extent to which the wedge flow field is dominated by coherent corner flow, the stronger the anisotropy and the larger δt . Conversely, for systems where the trench migrates rapidly compared with downdip motion, the wedge flow field is dominated by trench-parallel flow, and for rapidly moving trenches, δt is large as well. For subduction systems in the intermediate regime, the two flows compete, and the resulting flow field is less coherent. In such a situation, where the flow is weak or changes rapidly over short length scales, coherent and strong LPO does not develop (23) and δt is small.

Our model for wedge anisotropy may resolve the apparent conflict between studies that explain trench-parallel ϕ with trench-parallel flow (12, 10) versus with B-type olivine LPO (16, 21, 18). For subduction systems predicted to be dominated by corner flow, such as Ryukyu, the low-temperature conditions in the forearc are expected to favor the development of B-type LPO (17). For systems predicted to be dominated by trench-parallel flow, such as Tonga, we hypothesize that this flow regime increases overall velocities in the mantle wedge. This results in the removal of wedge material that has been conductively cooled by the slab, as found in laboratory models of subduction systems with rollback (24). The resulting higher forearc temperatures would favor A-type (or similar) rather than B-type LPO (6), so that ϕ close to the trench would reflect trench-parallel flow. For either type of subduction zone, farther away from the trench, ϕ should be trench-perpendicular, away from the influence of either the trench-parallel flow or B-type olivine fabric. This pattern is, indeed, observed in many subduction zones (25), including both Tonga and Ryukyu (12, 21). When this change in fast direction is controlled by a fabric transition, the change in orientation should coincide roughly with the arc (17); this would not necessarily be the case for systems with substantial trench-parallel flow. Again, this prediction is consistent with observations from end-member regions (12, 21).

Our model does not include possible effects on anisotropy due to aligned melt, lithospheric anisotropy in the overriding plate, crustal foundering, or trench-parallel flow due to oblique subduction. We have investigated whether splitting parameters correlate with the deformation regime of the overriding plate, subduction obliquity, volcanic production, and other parameters and find

Fig. 3. Average wedge δt versus $V_{\text{norm}} = (|V_t|/V_c)$ (trench velocity normalized by total convergence velocity). The x axis is plotted on a log scale. Retreating trenches are shown with blue diamonds, advancing trenches with red squares. Error bars roughly represent the 95% confidence region on average splitting times.

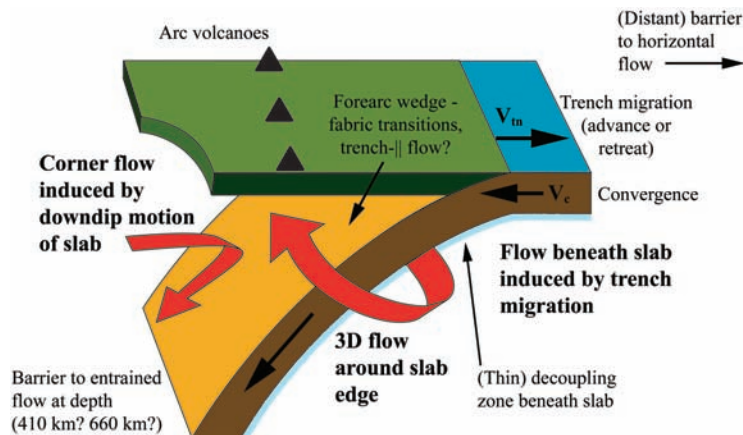
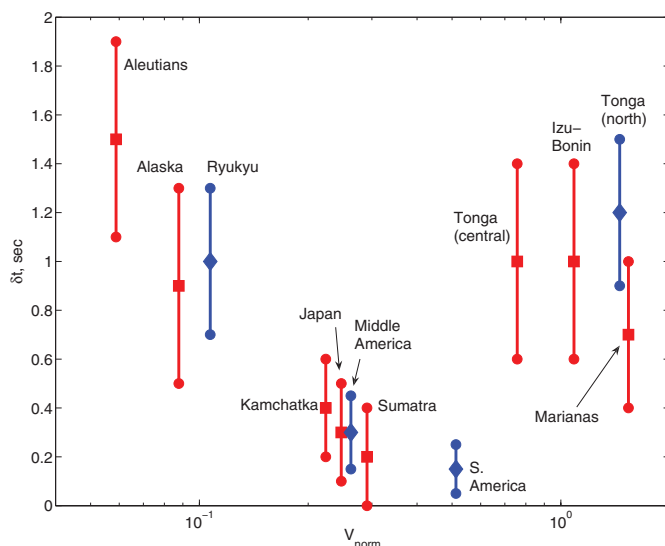


Fig. 4. Schematic diagram of model, showing the dominance of 3D flow beneath the slab and the competing influence of 2D and 3D flow fields in the mantle wedge.

no other notable global correlations. These effects may be important locally, but they do not represent a dominant global pattern. Additionally, we have not evaluated the possible effects of 3D slab morphology on trench-parallel flow in the wedge (e.g., 26) or beneath the slab (14, 27). Such flow is likely important locally and may serve to strengthen or otherwise modulate the trench-parallel flow induced by trench migration.

Our model essentially requires a thin decoupling zone between the downgoing slab and the subslab mantle, because we observe no detectable anisotropic signal from slab-entrained flow. [Cascadia represents an exception (8) to this rule; this may be a consequence of the very young age of the subducting lithosphere or the region's complicated subduction history and slab morphology.] This decoupling zone appears to be universal, in that slab-entrained flow is not generally detected even for subduction zones with a nearly stationary trench, and may be a consequence of the entrainment of a thin layer of buoyant asthenosphere (28). The inferred subslab flow field also requires a partial barrier to mantle flow beneath the slab, as proposed by (14), as well as an effective barrier to horizontal flow in the trench-normal direction (29), so that mantle material is forced to escape laterally in response to the motion of the trench. The barrier to entrained flow beneath the slab provides a constraint on mass transfer between the upper and lower mantle, which in turn has major implications for mantle evolution and dynamics. Finally, the existence of trench-parallel flow in the

mantle wedge as a common (although not ubiquitous) phenomenon implies that along-strike transport of mantle material is important for many arcs, with consequences for magma genesis, volatile transport, and thermal structure.

References and Notes

1. P. G. Silver, *Annu. Rev. Earth Planet. Sci.* **24**, 385 (1996).
2. M. K. Savage, *Rev. Geophys.* **37**, 65 (1999).
3. N. I. Christensen, *Geophys. J. R. Astron. Soc.* **76**, 89 (1984).
4. S. Zhang, S.-i. Karato, *Nature* **375**, 774 (1995).
5. H. Jung, S.-i. Karato, *Science* **293**, 1460 (2001).
6. H. Jung, I. Katayama, Z. Jiang, T. Hiraga, S. Karato, *Tectonophysics* **421**, 1 (2006).
7. M. J. Fouch, K. M. Fischer, *J. Geophys. Res.* **101**, 15987 (1996).
8. C. A. Currie, J. F. Cassidy, R. D. Hyndman, M. G. Bostock, *Geophys. J. Int.* **157**, 341 (2004).
9. M. D. Long, R. D. van der Hilst, *Phys. Earth Planet. Inter.* **151**, 206 (2005).
10. S. H. Pozgay, D. A. Wiens, J. A. Conder, H. Shiobara, H. Sugioka, *Geophys. J. Int.* **170**, 371 (2007).
11. C. Hall, K. M. Fischer, E. M. Parmentier, D. K. Blackman, *J. Geophys. Res.* **105**, 28009 (2000).
12. G. P. Smith *et al.*, *Science* **292**, 713 (2001).
13. M. D. Behn, G. Hirth, P. B. Keleman, *Science* **317**, 108 (2007).
14. R. M. Russo, P. G. Silver, *Science* **263**, 1105 (1994).
15. L. Mehl, B. R. Hacker, G. Hirth, P. G. Keleman, *J. Geophys. Res.* **108**, 10.1029/2002JB002233 (2003).
16. J. Nakajima, A. Hasegawa, *Earth Planet. Sci. Lett.* **225**, 365 (2004).
17. E. A. Kneller, P. E. van Keken, S.-i. Karato, J. Park, *Earth Planet. Sci. Lett.* **237**, 781 (2005).
18. M. D. Long, B. H. Hager, M. V. de Hoop, R. D. van der Hilst, *Geophys. J. Int.* **170**, 839 (2007).
19. A. Heuret, S. Lallemand, *Phys. Earth Planet. Inter.* **149**, 31 (2005).
20. E. M. Syracuse, G. A. Abers, *Geochem. Geophys. Geosyst.* **7**, 10.1029/2005GC001045 (2006).
21. M. D. Long, R. D. van der Hilst, *Phys. Earth Planet. Inter.* **155**, 300 (2006).
22. V. Levin, D. Droznin, J. Park, E. Gordeev, *Geophys. J. Int.* **158**, 1009 (2004).
23. É. Kaminski, N. M. Ribe, *Geochem. Geophys. Geosyst.* **3**, 10.1029/2001GC000222 (2002).
24. C. Kincaid, R. W. Griffiths, *Nature* **425**, 58 (2003).
25. Although the transition described here is more common, trench-perpendicular to trench-parallel transitions in ϕ have also been observed, for example, in Kamchatka and Alaska. These backward transitions are not easily explained by our model; however, because both Kamchatka and Alaska are located near slab edges, local processes may affect these regions.
26. E. A. Kneller, P. E. van Keken, *Nature* **450**, 1222 (2007).
27. J. Polet *et al.*, *J. Geophys. Res.* **105**, 6287 (2000).
28. J. Phipps Morgan, J. Hasenclever, M. Hort, L. Rüpke, E. M. Parmentier, *Terra Nova* **19**, 167 (2007).
29. L. Husson, C. Faccenna, C. P. Conrad, *Mem. Geosci. Montpellier* **41**, 169 (2007).
30. We thank the Alaska Regional Network, Alaska Tsunami Warning Seismic System, the Pacific Orient Seismic Digital Observation Network (POSEIDON), and the Incorporated Research Institutions for Seismology/United States Geological Survey for providing data used in this study. We thank M. Behn and S. Pozgay for useful discussions and L. Wagner for assistance with figures.

Supporting Online Material

www.sciencemag.org/cgi/content/full/319/5861/315/DC1
SOM Text
Figs. S1 to S5
References

21 September 2007; accepted 4 December 2007
10.1126/science.1150809

A Localized Negative Genetic Correlation Constrains Microevolution of Coat Color in Wild Sheep

J. Gratten,¹ A. J. Wilson,² A. F. McRae,³ D. Beraldi,² P. M. Visscher,³ J. M. Pemberton,² J. Slate¹

The evolutionary changes that occur over a small number of generations in natural populations often run counter to what is expected on the basis of the heritability of traits and the selective forces acting upon them. In Soay sheep, dark coat color is associated with large size, which is heritable and positively correlated with fitness, yet the frequency of dark sheep has decreased. This unexpected microevolutionary trend is explained by genetic linkage between the causal mutation underlying the color polymorphism and quantitative trait loci with antagonistic effects on size and fitness. As a consequence, homozygous dark sheep are large, but have reduced fitness relative to phenotypically indistinguishable dark heterozygotes and light sheep. This result demonstrates the importance of understanding the genetic basis of fitness variation when making predictions about the microevolutionary consequences of selection.

Evolutionary theory states that directional selection on a heritable trait should result in evolutionary change (1). Analyses of long-term data sets from wild vertebrate popula-

tions reveal directional selection on heritable traits, yet many studies report no microevolutionary change (stasis) or, in some cases, responses in the opposite direction to that predicted (2). Explaining such discrepancies is a major challenge in evolutionary biology (2). The absence of a predicted microevolutionary response may be due to constraints imposed by genetic correlations between the phenotype of interest

and other fitness-related traits (3). If this is true, then the loci affecting the focal trait should be colocalized in the genome with genes for other fitness-related traits, either because the same genes affect both traits (pleiotropy) or because genetic correlations arise between tightly linked genes (linkage disequilibrium). However, empirical evidence for colocalized antagonistically acting quantitative trait loci (QTLs) that constrain microevolutionary change is currently lacking.

In the free-living Soay sheep of St Kilda, Scotland, coat color is either dark brown or light tawny (Fig. 1) (4); the two phenotypes have been documented for at least 90 years (5, 6). Variation in coat color is controlled by a single autosomal locus at which the dark allele is dominant to the light allele (6). The light phenotype is determined by homozygosity of a single recessive amino acid-changing G→T transversion at coding position 869 in the *tyrosinase-related protein 1 (TYRP1)* gene (7).

Coat color in Soay sheep is related to fitness because of an association with body size: Dark sheep are larger than light sheep (8). Body size is heritable throughout life (9, 10) and is positively correlated with survival (11) and reproductive success (12). Moreover, a genetic response to selection for increased size has been detected (9). If the association between coat color and body

¹Department of Animal and Plant Sciences, University of Sheffield, Sheffield S10 2TN, UK. ²Institute of Evolutionary Biology, School of Biological Sciences, University of Edinburgh, Edinburgh EH9 3JT, UK. ³Genetic Epidemiology, Queensland Institute of Medical Research, Brisbane 4029, Australia.